Competing growth processes induced by next-nearest-neighbor interactions: Effects on meandering wavelength and stiffness

Sonia Blel,[1] Ajmi BH. Hamouda,[1,2,*] B. Mahjoub,[1] and T. L. Einstein[2,3]
[1]*Quantum Physics Laboratory, Faculty of Science, University of Monastir, Monastir 5019, Tunisia*
[2]*Department of Physics, University of Maryland, College Park, Maryland 20742-4111, USA*
[3]*CMTC, University of Maryland, College Park, Maryland 20742-4111, USA*
(Received 23 July 2016; revised manuscript received 8 December 2016; published 6 February 2017)

In this paper we explore the meandering instability of vicinal steps with a kinetic Monte Carlo simulations (kMC) model including the attractive next-nearest-neighbor (NNN) interactions. kMC simulations show that increase of the NNN interaction strength leads to considerable reduction of the meandering wavelength and to weaker dependence of the wavelength on the deposition rate F. The dependences of the meandering wavelength on the temperature and the deposition rate obtained with simulations are in good quantitative agreement with the experimental result on the meandering instability of Cu(0 2 24) [T. Maroutian *et al.*, Phys. Rev. B **64**, 165401 (2001)]. The effective step stiffness is found to depend not only on the strength of NNN interactions and the Ehrlich-Schwoebel barrier, but also on F. We argue that attractive NNN interactions intensify the incorporation of adatoms at step edges and enhance step roughening. Competition between NNN and nearest-neighbor interactions results in an alternative form of meandering instability which we call "roughening-limited" growth, rather than attachment-detachment-limited growth that governs the Bales-Zangwill instability. The computed effective wavelength and the effective stiffness behave as $\lambda_{\rm eff} \sim F^{-q}$ and $\tilde{\beta}_{\rm eff} \sim F^{-p}$, respectively, with $q \approx p/2$.

DOI: 10.1103/PhysRevB.95.085404

I. INTRODUCTION

Thin-film growth processes involve many different types of kinetics giving rise to a variety of surface morphologies. Experimental and theoretical investigations carried for different materials and a broad temperature range revealed that island nucleation (or 3D growth) is the dominant mechanism ([1] and references therein). However, at relatively low deposition rate on vicinal surfaces, two-dimensional (2D) "step flow" growth takes place, with the morphology evolving towards many different nonequilibrium structures. Such structures are found to be governed essentially by surface diffusion and mass transport, both on the surface terraces and at step edges. Many other mechanisms have been proposed in the literature [2–4] that may play a more or less important role in structuring the surface and governing their morphology.

In this paper, we are concerned with a well-known feature of surface morphology, the meandering instability. This form of instability, specifically its characteristic wavelength, has been studied extensively, particularly in the context of the Bales-Zangwill (BZ) picture. Continued theoretical work has been spurred by the instability of BZ theory to account for the observations in classic investigations of vicinal copper by Ernst's group [5–7]. This has led to the discovery of alternative mechanisms for the formation of a meandering, as well as of a mounding, instability [3,4].

In conventional materials, the nearest-neighbor (NN) interaction strength is found to be dominant [8]. Hence, either for that reason or for simplicity and clarity, most theoretical studies and simulation models usually neglect further interactions. However, on a surface lattice with square symmetry, the assumption of just NN interactions leads to idiosyncratic fluctuations of steps in non-close-packed orientations, since many different paths have the same rectilinear L_1 distance ("Manhattan" or "city block") and so give a large degeneracy. The simplest way to remedy this anomalous behavior is to include a next-nearest-neighbor "NNN" interaction, although trio (three-atom, nonpairwise) interactions and others could also serve this function. Here, we investigate how NNN interactions (in particular, attractive ones) compete with NN ones and alter the wavelength of the meandering instability of steps.

In addition to their effect on the surface morphology (i.e., the instability), we also consider the effect of the NNN interactions on step dynamics—more precisely, on step stiffness and adatom mobility. The resulting surface morphology, specifically in the step-flow-growth regime, is strongly governed by the step motion (or velocity) and the energetic cost of step bending (local curvature energy). Indeed, the step dynamics is the result of interplay between two processes that occur on terraces and at step edges. The physics on terraces is controlled by the adatom concentration or the adatom mobility on terraces. At step edges, in contrast, the step stiffness and the adatom mobility determine such properties as step anisotropy, Ehrlich-Schwoebel (ES) barrier, and kink ES barrier; their effect translates into effective boundary conditions on the *adatom density* (or *mobility*) field.

The paper is divided into five sections. The computational details of our kMC model are described in Sec. II. Section III is devoted to a brief comparison between the theoretical and experimental results of the meandering wavelength. Then our simulation results are presented in Sec. IV, where the previous effective quantities (wavelength and stiffness) are computed as functions of the deposition rate F, and their behavior is discussed for different NNN interaction strengths. Conclusions are provided in Sec. V.

II. COMPUTATIONAL DETAILS

The principles of our simulation model can be found elsewhere [9–12]. We focus on the effect of the deposition

*ajmi.hammouda@fsm.rnu.tn

 ©2017 American Physical Society

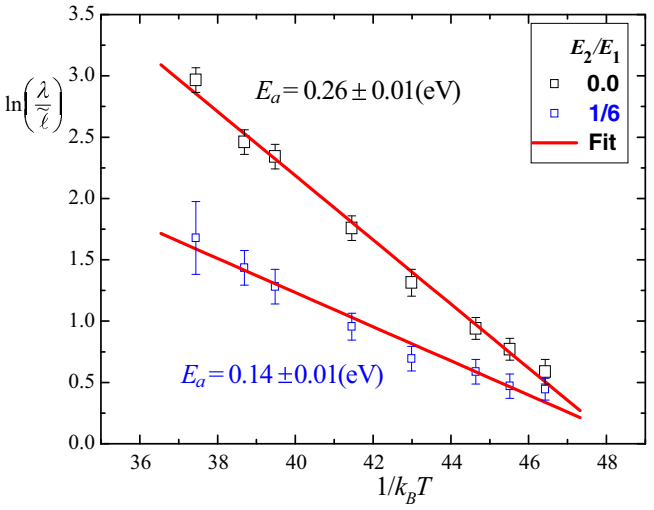

FIG. 1. Natural log of effective wavelength vs inverse growth temperature at $F = 3 \times 10^{-3}$ ML/s, $T = 250{-}310$ K, for vanishing and finite NNN interactions E_2. The wavelength takes the form $\lambda_{\text{eff}} = \lambda_0 \exp(-E_a/k_BT)$, where λ_0 is a constant and E_a is the activation energy.

rate on vicinal surfaces, with asymmetric step attachment (arising from the ES barrier [13] at step edges) with energy $E_{\text{ES}} = 0.07$ eV. We carried out extensive simulations on stepped surfaces of size $1000a \times 100a$. In the same spirit as Refs. [9,11], our kMC simulation model used a standard solid-on-solid model on a simple-cubic model rather than an fcc template, with lattice spacing a, containing ten steps initially perfectly straight, extending 1000 units in the x direction, and with dimensionless terrace width $\tilde{\ell} = 10$ (expressed in units of a). In the presence of an ES barrier, step fluctuations lead after a few monolayers of growth to the appearance of the meandering instability in the direction y perpendicular to steps. The surface height h (in the z direction, normal to the terraces) is a single-value function, so overhangs are forbidden, but single vacancies can form temporarily.[1] After long-time growth, digs of varying depth may be observed between the meanders depending on the deposition rate. The deposited atoms diffuse on the surface, with desorption forbidden, corresponding to the assumptions of molecular beam epitaxy (MBE). Periodic and screw-periodic boundary conditions are assumed in the x and y directions, respectively. The growth temperature is fixed at $T = 280$ K (except for results of Fig. 1, where the temperature is varied between 250 and 310 K at fixed flux), and the deposition flux was varied between $F = 5 \times 10^{-4}$ and 2×10^{-2} ML/s, where ML denotes monolayers. These rates span the range from a barely perceptible effect (small step fluctuations) to the verge of the meandering instability that announces the crossover from 2D step-flow growth to 3D mound growth.

[1]In early growth, vacancies (in 2D) may form temporarily (until the site is revisited) in the vicinity of steps due to the formation of fractal structures caused by NNN interactions, as well as 3D holes in later growth.

The NN bonding energy is fixed at $E_1 = 0.26$ eV throughout our simulations, while the NNN interaction energy E_2 (included in our simulations) is used as an independent parameter that is varied between 0 and $E_1/2$, with particular attention devoted to $E_2 = (1/6)E_1 = 0.043$ eV [8]. Once deposited on the surface, adatoms diffuse with a hopping barrier $E = E_d + n_1E_1 + (n_2E_2 + E_{\text{ES}})$, where $E_d = 0.4$ eV is the diffusion barrier for free adatoms and n_1 and n_2 are, respectively, the number of nearest- and next-nearest-neighbor adatoms before hopping ($n_1,n_2 = 0,1,2,3,4$). This amounts to assuming a constant height for the diffusion barrier energy and an initial state determined by bond counting. The attempt frequency is set to $\nu_0 = 10^{13}$ s^{-1}. We note that all of these parameters are exactly or nearly representative of the experiment in Refs. [5–7] and in the range of the theoretical predictions of Refs. [9,14] for E_d, Refs. [15,16] for E_1, and Refs. [17–21] for E_{ES}.

Our simulation results were directly compared to the experiment of Ref. [5], for Cu(0 2 24) ($\langle 001\rangle$ step edges), in which the mean terrace width is (2.17 ± 0.05) nm, corresponding to a dimensionless length $\tilde{\ell}_{\text{exp}} \approx 8.5 \pm 0.2$ (given the interatomic Cu distance $a = 0.255$ nm), slightly lower than the value we used. The temperature ranges between 250 and 400 K, and the flux between 8×10^{-4} and 10^{-2} ML/s (see Figs. 4 and 5 of Ref. [5]). The effective meandering wavelength λ_{eff} and the step stiffness $\tilde{\beta}_{\text{eff}}$ are computed as functions of the deposition rate and for several NNN interaction strengths, while an effective adatom mobility σ_{eff} can be defined from the two previous quantities.[2]

III. THEORETICAL PREDICTIONS VS EXPERIMENTAL RESULTS FOR COPPER

As noted above, our goal in this paper is to cleanly investigate theoretically a simple mechanism (the NNN interaction) that lifts the Manhattan-length degeneracy of steps on a square lattice in non-close-packed directions. NNN interactions are often intentionally neglected, but their effect could be crucial or at least among the most effective mechanisms for step dynamics—and consequently on the meandering instability, as we will see for the case of copper. Kinetic Monte Carlo (kMC) is well suited for this kind of study [22]. Before presenting our kMC results, we summarize the main results concerning the meandering instability.

The BZ theory predicts an instability wavelength that varies with the deposition flux as $\lambda_{\text{BZ}} \propto F^{-q}$, where the exponent $q = 1/2$. This prediction is confirmed by kMC simulations of step meandering with an ES barrier [19,23] as well as in our own simulations [9,11]. However, an in-plane variant microscopic mechanism, spawned by asymmetric incorporation into kinks (the kink-Ehrlich-Schwoebel effect (KESE) [3,24], leads to the prediction that the wavelength of

[2]The exact measurement of the mobility of adatoms is not straightforward; nevertheless, from the knowledge of the effective wavelength and stiffness, we can define a quantity which has the dimension of an effective mobility as follows: $\sigma_{\text{eff}} \propto (\lambda^2{}_{\text{eff}}F/\tilde{\beta}_{\text{eff}})$, independent computation of the latter is, of course, required for better understanding of the role of mobility on the wavelength limitation.

the instability varies as $\lambda_m \propto F^{-1/4}$, in better agreement with experiments and in disagreement with the prediction of BZ theory.

On the other hand, Ernst's group's experimental STM results yielded $\lambda_{100} \cong 1.55 \times F^{-(0.17\pm0.09)}$ for Cu(0 2 24) and $\lambda_{110} \cong 2.18 \times F^{-(0.21\pm0.08)}$ for Cu(1 1 17), where steps are oriented in the open ⟨100⟩ direction and the close-packed ⟨110⟩ direction, respectively. They also showed that when deposition is continued beyond 10 ML at higher flux ($F > 10^{-2}$ ML/s), relatively regular square-base pyramids appear on the meanders. This obvious disagreement of the exponent q with the prediction of BZ has stimulated much theoretical work (for more details, see Refs. [9,23]).

In recent years some of us have also explored the effect of an extrinsic component, specifically, some kind of codeposited impurity on the structuring of stepped surfaces and the meandering wavelength [9,11,25]. Indeed, codeposited impurities during growth are known to have remarkably great influence on surface morphology, even in small amounts, and may also serve as a nanostructuring tool ([26] and references therein). They are shown to produce quantitative and qualitative changes in the surface morphology. In particular, impurities make adatom diffusion less dependent on the deposition rate, affecting thus the wavelength of the meanders and, consequently, alleviating the previous disagreement and partially explaining the experimentally observed features (appearance of pyramids). Indeed, impurities are shown to act as nucleation centers, causing the observed small pyramids to form on the surface. On the one hand, the diffusion of adatoms (and so their mobility) obviously may be impeded by the deposition rate, analogous to the effect of impurities. On the other hand, the NNN interactions may also hinder adatom diffusion, thereby decreasing both their mobility and the step stiffness.

According to the theoretical model of Bales-Zangwill and starting from a linear stability analysis of a growing stepped surface, the fastest growing mode is found to be the in-phase mode with a wavelength that can be written in terms of the equilibrium stiffness and adatom mobility [5,7,17,19,20,27–30]:

$$\lambda_{\mathrm{BZ}} = 4\pi \sqrt{\frac{a^4 \tilde{\beta}^{\mathrm{eq}} \left(\sigma_s^{\mathrm{eq}} + \sigma_T^{\mathrm{eq}}\right)}{f_{\mathrm{ES}} \ell^2 F}}, \tag{1}$$

where the strength of the ES barrier appears in the factor f_{ES}. The term in parentheses is the equilibrium total mobility σ^{eq}, which is a sum of two terms: the mobility of adatoms on the terraces σ_T^{eq}, corresponding to the mass transfer (or relaxations) via terraces diffusion, and the mobility of adatoms at the steps σ_s^{eq}, corresponding to the relaxation via step-edge diffusion. The driving force of both of these mass currents is the gradient of the step chemical potential. The mobility of adatoms on terraces is $\sigma_T^{\mathrm{eq}} = \frac{\ell D_T c_T^{\mathrm{eq}}}{k_B T}$ [19,20,23,31], where D_T is the terrace diffusion constant, c_T^{eq} the adatom concentration on the terrace. The mobility along step edges is assumed to have a similar form: $\sigma_s^{\mathrm{eq}} = \frac{a D_s c_s^{\mathrm{eq}}}{k_B T}$. This latter may be neglected under several conditions.[3] We emphasize here that Eq. (1) is valid at equilibrium; it contains the "equilibrium" step stiffness and the adatom mobility. One can also measure the same quantity during deposition; therefore, all these quantities we measured from our simulations are "effective" nonequilibrium ones and should, eventually, depend on deposition rate F; this is the main assumption of the present study and its accuracy will be tested by comparison of results from our kMC simulations to those from heuristic expectations deduced from available theoretical models. To better grasp our assumption, one must bear in mind that the measured quantities can be affected by intrinsic effects (notably in our study, NNN interactions), much as they can be affected by extrinsic effects, such as impurities, and their values should deviate from those at equilibrium. Therefore, we distinguish between the original BZ instability (fundamentally caused by step anisotropy or the ES barrier) and the BZ instability affected by any other mechanism (NNN, impurities, etc.); in the last case, we talk about "effective quantities." Note that in our case the NNN effects are in the barriers of the kMC model, and so affect the evolution under deposition and contribute to nonequilibrium coefficients. When NNN interactions just enter in the lattice gas energies, they contribute to the equilibrium stiffness, etc., as in Ref. [32].

Henceforth, we assume that both the effective step stiffness $\tilde{\beta}_{\mathrm{eff}}$ and the effective adatom mobility σ_{eff} are affected by the NNN interactions strength, consequently affecting the wavelength of the meandering instability. The exact dependence of the latter quantities on the deposition rate F and on the NNN interactions strength will be detailed in the next section.

IV. SIMULATION RESULTS

A. Wavelength of the meandering

In Fig. 1 the meandering wavelength is plotted vs the inverse temperature (in semilog Arrhenius fashion, $\lambda_{\mathrm{eff}} = \lambda_0 \exp(-E_a/k_B T)$) at fixed flux $F = 3 \times 10^{-3}$ ML/s. The thermal activation energy of the meandering wavelength is found to be $E_a = (0.26 \pm 0.01)$ eV at $E_2 = 0$, i.e., roughly equals E_1 (which should be the thermal activation energy for the BZ instability) and decreases with NNN interactions to $E_a = (0.14 \pm 0.01)$ eV ($\approx E_1/2 \approx E_1 - 3E_2$)[4] at

[3] The concentration of the edge adatoms, i.e., adatoms having lateral bonds with the step edge, may be nearly independent of deposition rate F due to the intensive exchange, enhanced by NNN interactions, between the edge adatoms and the atoms in the kink positions. However, the solution of the surface diffusion equation subject to the kinetic boundary conditions, such as Eq. (6) in Ref. [29], shows that the adatom concentration depends on F even in the vicinity of the step edge.

[4] In equilibrium the attachment-detachment process is the mechanism limiting step fluctuation. However, in growth, the attachment is the limiting process, which is enhanced with NNN interactions, making the process seemingly more complicated. Indeed, the best fit is rather exponential, $E_a \approx E_1 \times \exp(-3 \times E_2/E_1)$; then $E_a \approx E_1 - 3 \times E_2$ is a good approximation for $E_2 < E_1/6$. We are not able to justify definitively this result, but the limiting process could be the attachment of a free adatom from the terrace (from the incoming flux) to a kink position of height 2 (which is a more stable position than attachment into a step edge or into a simple kink of height 1).

TABLE I. Prefactor C_{kMC} and exponent q of the effective wavelength vs NNN interaction strength E_2, extracted from the best fit to kMC data plotted in Fig. 2.

E_2/E_1	C_{kMC}	q
0	**0.434 ± 0.046**	**0.447 ± 0.015**
1/25	0.587 ± 0.036	0.346 ± 0.009
1/20	0.605 ± 0.049	0.331 ± 0.012
1/15	0.652 ± 0.057	0.307 ± 0.013
1/12	0.710 ± 0.040	0.274 ± 0.008
1/10	0.752 ± 0.050	0.253 ± 0.010
1/8	0.778 ± 0.051	0.225 ± 0.010
1/6	**0.952 ± 0.055**	**0.167 ± 0.009**
1/4	1.245 ± 0.049	0.095 ± 0.006
1/2	1.509 ± 0.091	0.036 ± 0.010

$E_2 = (1/6)E_1$. The latter is in good agreement with the experimental result, $E_{\mathrm{exp}} = (0.132 \pm 0.012)$ eV [5,17].

In Fig. 2 the meandering wavelength is plotted vs flux for different NNN interaction strengths E_2, at fixed temperature $T = 280$ K. As we can see, for all E_2 values, λ decreases with F in a power-law fashion, with an exponent q that decreases from $q = 0.45$ at $E_2 = 0$ to a very small value (implying weak F dependence) with increasing E_2. In particular, for $E_2 = (1/6)E_1$ we found $q_{\mathrm{kMC}} = 0.167 \pm 0.009$ (see Table I). This exponent q is nearly the value found in the experiment of Maroutian *et al.* for Cu(0 2 24) at $T = 294$ K [5]. However, the prefactor $C_{\mathrm{kMC}} = 0.952 \pm 0.055$ (see Table I) is much lower than the experiment ($C_{\mathrm{exp}} = 1.55$). Indeed, in order to match our simulation results with the experiment, we should rescale the temperature and the terrace width to our simulation values. From Fig. 4 of Ref. [5], we can easily extract the experimental wavelength corresponding to our temperature ($T = 280\,\mathrm{K} \rightarrow 1000/T = 3.57\,\mathrm{K}^{-1}$) and for $F = 3 \times 10^{-3}$ ML/s, we find $(\lambda/\tilde{\ell})_{\mathrm{exp}} \approx 3 = C_{\mathrm{exp}} \times (3 \times 10^{-3})^{-0.17}$, so $C_{\mathrm{exp}} = 1.12$, and then $(\lambda/\tilde{\ell})_{\mathrm{exp}} = 1.12 \times F^{-0.17}$. Rescaling the experimental mean terrace width $\tilde{\ell}_{\mathrm{exp}} \cong 8.5$ to our value $\tilde{\ell} = 10$ yields $(\lambda/10)_{\mathrm{exp}} = (8.5/10) \times 1.12 \times F^{-0.17} = 0.95 \times F^{-0.17}$, which is in excellent agreement with our simulation values found for $E_2 = (1/6)E_1$ (see Table I). This energy is, indeed, the NNN bonding strength computed theoretically in Ref. [8].

The rescaling to the experimental temperature and terrace width is a common numerical manipulation. This is arguably the most remarkable agreement between the experiment and our simulations found in this study, strongly supporting the validity of our model. The latter seemingly takes into account the most important effective processes in the studied system and confirms the ability of our simulations to reproduce the experimental results over the experimental temperature range.

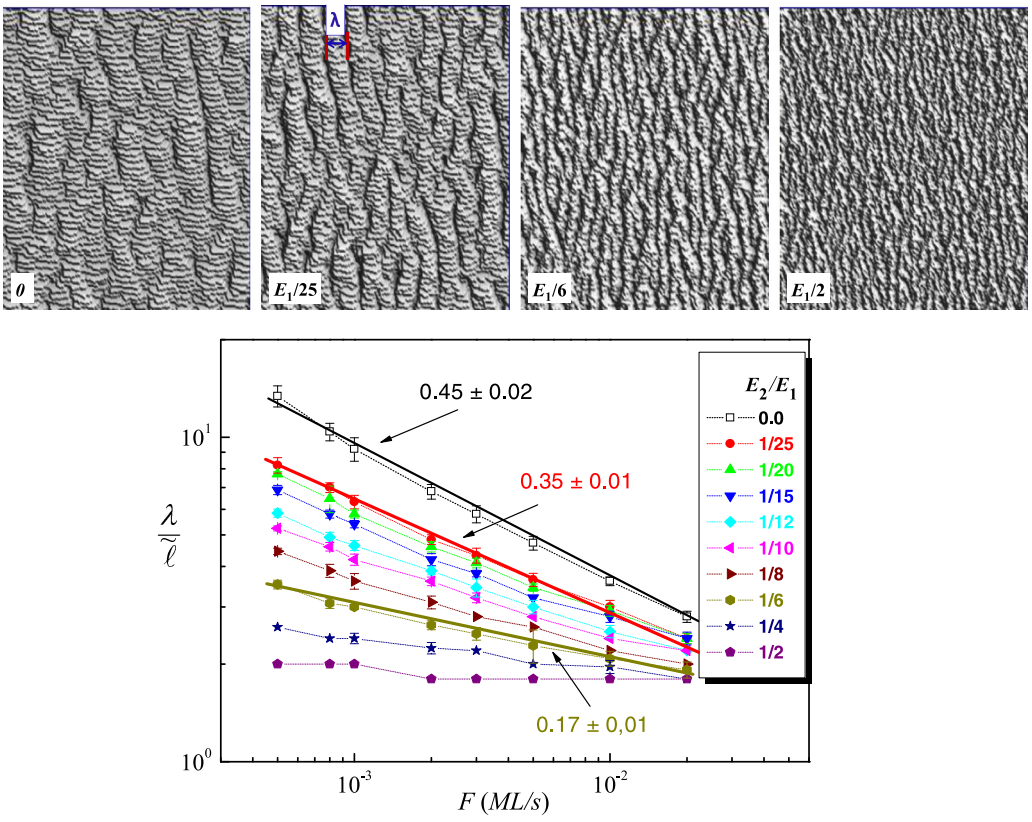

FIG. 2. (Upper) Snapshots of the simulated surface (segment of 500 × 500 sites shown) at $F = 2 \times 10^{-3}$ ML/s and for different NNN interactions bonding energy value E_2 after growth of 20 ML. Steps are evolving from top to bottom of the images; i.e., the terraces at the top are higher than those at the bottom. (Lower) Meandering wavelength vs deposition rate with increasing NNN interaction strength (E_2/E_1). The measured wavelength is the mean of all meander widths. Error bars are obtained over ten independent simulations. The wavelength follows a power law: $\lambda_{\mathrm{eff}} \sim C_{\mathrm{kMC}} \times F^{-q}$ (in agreement with BZ theory), where the prefactor C_{kMC} and the exponent q are found to depend on the NNN energy E_2. The flux is varied between 5×10^{-4} and 2×10^{-2} ML/s at $T = 280$ K and with $E_{\mathrm{ES}} = 0.07$ eV.

To summarize, we found excellent quantitative agreement with the experiment, not only for the exponent $q = 0.17$ when $E_2 = (1/6)E_1$, but also for the prefactor $C_{\rm exp} = 1.55$. The latter agreement confirms that our simulations are reproducible at the range of temperature where the meandering instability develops, estimated between 250 and 320 K in our simulations.

Our results could be interpreted as follows: The meandering instability seems to be sensitive to even small perturbations, specifically NNN interactions but also small concentrations of impurities, affecting the dynamics of steps and surface diffusion of adatoms. These effects are manifested in the instability-wavelength behavior. Particularly, the latter is found to be very sensitive to attractive NNN interactions and presumably to any more complicated mechanism that lifts the degeneracy of Manhattan path lengths of steps. In our context, NNN interactions increase step fluctuations and cause fractal fingers to form at the step edge. These fractal shapes drastically affect the effective step stiffness, competing with the meandering instability, decreasing both the stiffness and the instability wavelength as strength of the NNN interactions increases.

Indeed, in the submonolayer regime, the islands growing on nominal surfaces have nearly smooth step edges (compact islands) for vanishing E_2, but for $E_2 > E_1/6$, very rough island edges are observed in simulations, exhibiting numerous bifurcations (fingers) which look like fractals at the highest NNN values. These fractal fingers cease to grow, thereafter decreasing the meandering wavelength. This reasoning is confirmed by recent work on island size distributions in models of submonolayer surface growth [33]. The latter showed that fractal morphologies exhibit a lower coalescence rate than compact ones caused by the fact that fingers of two approaching fractal islands typically first avoid each other, which subsequently leads to a screening effect and a slowing down of further growth of these fingers.

Now we focus on why both impurities and NNN interactions lead to similar behavior of the wavelength dependence on deposition rate. Besides the effects of NNN or similar symmetry-breaking interactions, the instability behavior may be affected by nucleation mechanisms, as reported in Ref. [9] and recently in Ref. [34]. Indeed, the presence of 2D islands influences step-flow growth; moreover, the coalescence of such islands with neighboring steps can modify the wavelength of the meandering transition from step flow to 3D layer-by-layer growth. During this transition, 2D nucleation and island coalescence significantly modify the meandering instability from the well-known BZ instability to a different "form" of instability—the nucleation and coalescence meandering instability [34].

In our case, when we increase the NNN interactions, one can expect that the growth process switches over to the step-roughening mechanism (or nucleation for impurities), which might produce a dependence of the effective stiffness on the deposition rate essentially similar to that in the impurities case (Ref. [9]); this similarity is illustrated in Fig. 3. This is why the NNN interaction strength can be seen to act like an effective impurity concentration—the higher the interaction, the more effective adatoms are as "traps" (and the more impurities, the more traps there are). Thus, what sets the length scale of the instability is step roughening (as it is nucleation for impurities), which is presumably the main aspect that NNN affects. Indeed with NNN interactions, the effective "size" of an adatom is extended, that can now capture other diffusing adatoms not only when they are NN, but also when they are NNN. When we further increase the interaction strength, the step roughness becomes ever less dependent of the deposition rate, because atoms simply stick where they touch the step and do not move anymore and the steps are progressively more ramified. Therefore, in the spirit of Ref. [34], we obtain a different form of meandering instability—the roughening-limited growth, which is simply the BZ instability altered by NNN interactions.

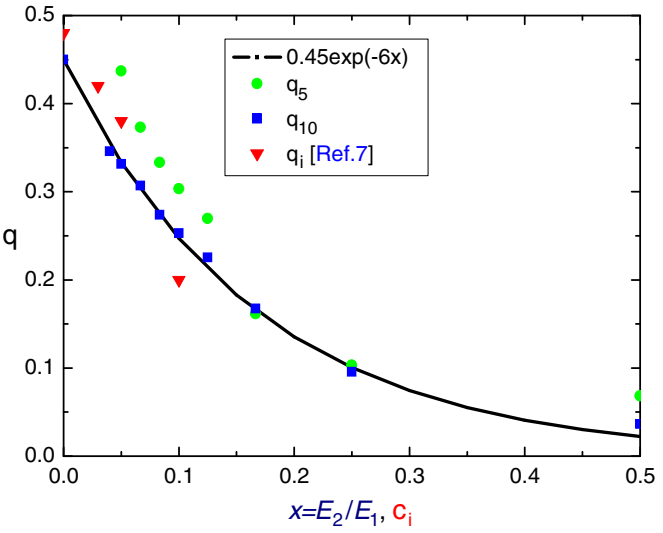

FIG. 3. Plot of the exponent q vs the ratio $x = (E_2/E_1)$ at fixed E_1 for $\tilde{\ell} = 10$ (blue squares). For purpose of comparison, we show the data for $\tilde{\ell} = 5$ (green circles, where finite-size effects could explain the mediocre accuracy of some points), and also the result found in Ref. [9] where c_i is the concentration of impurities (red triangles). The dark solid line is the best fit of the overall data to an exponential decay.

In conclusion, the introduction of NNN interactions into the system affects the meandering wavelength, decreasing its dependence on the deposition rate F. The exponent q in the $\lambda - F$ relationship decays exponentially with the NNN interaction, the best fit giving (Fig. 3):

$$q(E_2) \approx (0.45 \pm 0.02)\exp[-(6.0 \pm 0.2)E_2/E_1] \approx (1/2)\exp(-E_2/2k_BT). \quad (2)$$

From the latter equation, we can see that for vanishing NNN interactions, $q = 1/2$, which is the BZ prediction, whereas for a particular finite NNN strength ($E_2 = (1/6)E_1$), $q = 0.16$, just as in the experimental results. In Fig. 3, the behavior for each set of points for small x looks almost linear; for small E_2, one can write $q(E_2) \approx 0.45 \times (1 - 6E_2/E_1)$.

Even though the meandering instability has been extensively studied over the last three decades, the disagreement between the experiment and current theories remains unresolved. Here, we present a mechanism (NNN interactions) that accounts for the disagreement. This finding should stimulate more theoretical models of step instabilities.

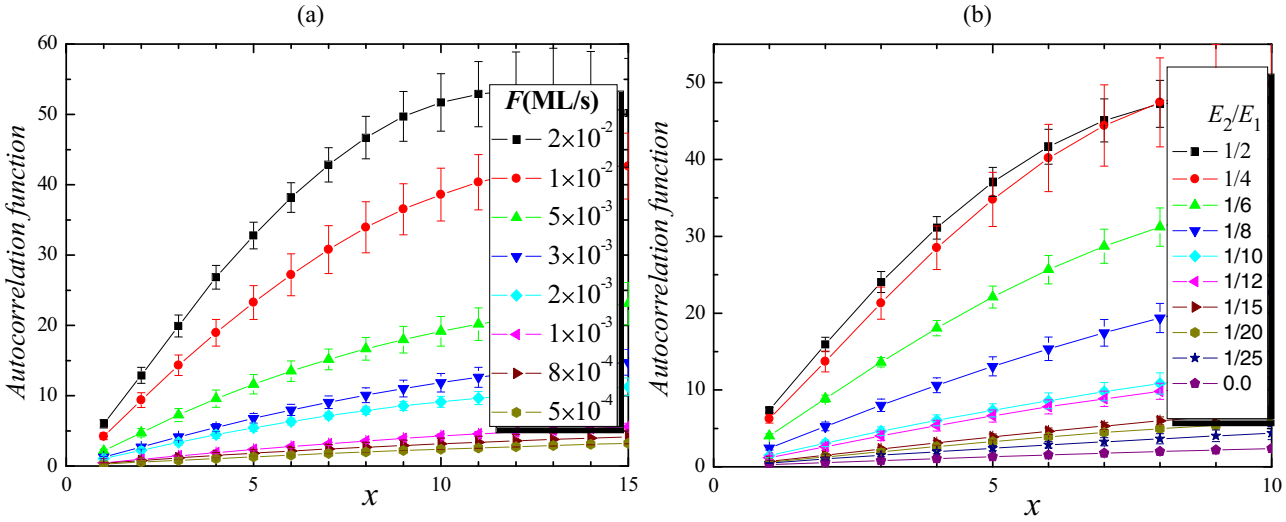

FIG. 4. Autocorrelation function of the step profile $y(x)$: (a) for various flux, at fixed $E_2 = 0$ and (b) for various E_2/E_1 values, at fixed $F = 5 \times 10^{-4}$ ML/s, $E_{ES} = 0.07$ eV, and $T = 280$ K. Error bars are obtained over ten simulations.

B. Effective stiffness

Within the solid-on-solid (SOS) approximation, Stasevich *et al.* [32,35] demonstrated the equilibrium dependence of the step stiffness on NNN interactions for Cu(001). Mehl *et al.* [8] found that energy barriers are not simply the sum of bond energies, so that the NNN bonding energy deduced from a set of such barriers depends on the diffusion path (i.e., on the local configuration of adatoms). On all the (001) surfaces that they checked (Ag, Au, Ni, and Pd), except for Cu, the inclusion of a nonlinear term in the total hopping energy is much larger than the NNN bond, sometimes by an order of magnitude. Therefore, Cu is the best material to check for the effect of NNN interaction strength on the stiffness and then on the meandering wavelength.

In this section, we show that the effective stiffness exhibits a similar flux dependence as the meandering wavelength. Since NNN interactions affect, in particular, the kinetics near step edges, the effective stiffness should be also affected. Because the latter is proportional to the instability wavelength in a power-law fashion, one expects that any change of the former with NNN interactions will modify the latter one. Indeed, the effective stiffness is related to the in-plane-autocorrelation function $g_y(x)$ along the step edges at small separation x (see Fig. 4), which reads [36,37]

$$g_y(x) = \langle [y(x+x') - y(x')]^2 \rangle \approx \frac{k_B T}{a\tilde{\beta}_{\text{eff}}} a|x|, \qquad (3)$$

where, again, x is the coordinate running parallel to the mean step-edge direction and y is the in-plane perpendicular coordinate. The effective stiffness is then extracted from the coefficient of $|x|$ in Eq. (3). In Fig. 5, we have plotted the effective stiffness vs flux for different energetic barriers. It is found to follow the same trend vs flux as the effective wavelength ($\tilde{\beta}_{\text{eff}} \sim F^{-p}$ where $\lambda_{\text{eff}} \sim F^{-q}$), but with a power-law exponent p nearly twice as large as q.

Furthermore, in our range of flux and for the unstable regime (i.e., for $E_{ES} = 0.07$ eV, red (with circles) and blue (with downward-pointing triangles) lines in Fig. 5), the stiffness decreases fairly rapidly with NNN interaction strength and vanishes at higher flux, where there is a crossover from meandering to island instability. This decrease is, however, much slower for the stable regime (i.e., for $E_{ES} = 0$ eV, black (with squares) and green (with upward-pointing triangles) lines in Fig. 5); the effective stiffness maintains a finite value even at higher flux.

Focusing on the unstable regime, where the meandering instability is observed, one can note that the effective stiffness exponent is $p = (0.95 \pm 0.01) \approx 1$ (red data in Fig. 5) at $E_2 = 0$, corresponding to $q = (0.45 \pm 0.02) \approx 1/2$ (as predicted in the BZ theory) and $p = (0.33 \pm 0.01) \approx 1/3$ (blue data in Fig. 5) at $E_2 = (1/6)E_1$, corresponding to $q = (0.17 \pm 0.01) \approx 1/6$ (as found in the experiment). Thus, in both cases, one can write, to good approximation, $p = 2q$.

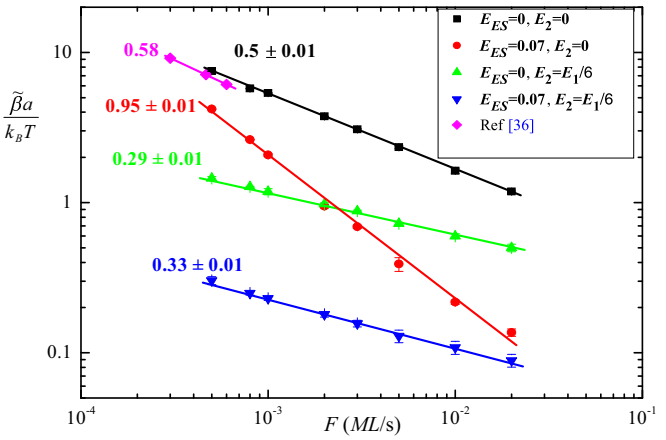

FIG. 5. Effective stiffness vs deposition rate F, at $T = 280$ K for different energetic barriers E_{ES} (in eV) and E_2. The three diamond points are extracted from Ref. [36] and plotted for comparison. The simulation data (symbols) are fitted (solid line) with linear function in the log-log plot $\tilde{\beta}_{\text{eff}} \sim F^{-p}$; the slope p is listed for each fit.

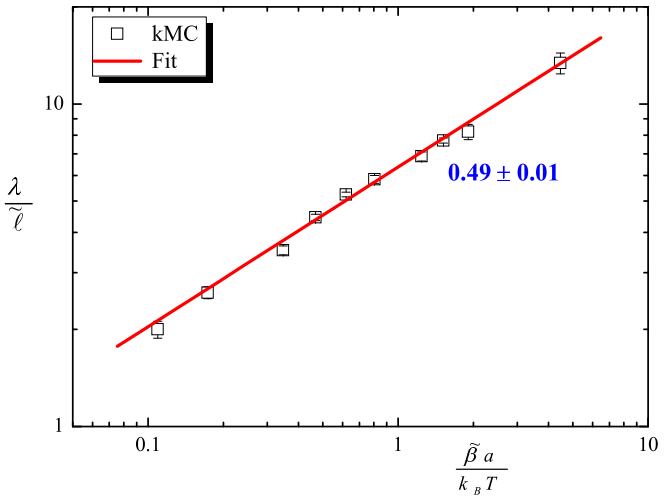

FIG. 6. Effective wavelength vs effective stiffness at $T = 280$ K, and after 20 ML of growth, $\lambda_{\rm eff}/\tilde{\ell} \sim \tilde{\beta}_{\rm eff}^{1/2}$.

In the stable regime ($E_{\rm ES} = 0$, no meandering instability), we compute $p = (0.50 \pm 0.01)$, in perfect agreement with a heuristic deduction[5] of the exponent $p = 1/2$ [black (with squares) data in Fig. 5] with only NN interactions. Our results also agree relatively well with Ref. [36], where we have extracted the exponent $p = 0.58$. Thus, the effective stiffness depends not only on the energetics at the step edge, but also on the deposition rate. Note that at a given deposition rate, only the amplitude of the effective stiffness depends on the ES barrier; however, the exponent p (therefore q) depends on the NNN strength E_2.

When the effective wavelength is plotted vs the effective stiffness (Fig. 6), we found $\lambda_{\rm eff} \sim \tilde{\beta}_{\rm eff}^{(0.49\pm0.01)}$, in good agreement with Ref. [38]. This behavior is again reminiscent of the BZ theory for equilibrium quantities [Eq. (1)].

In conclusion, as we increase the strength of NNN interactions, nucleation at steps and consequent discursions progressively increase (on flat surfaces, the nucleated islands evolve from compact to fractals), thereby increasing the number of kinks. Hence, the attachment process of adatoms into steps is enhanced, leading to a smaller effective stiffness, as well as a weaker dependence on the deposition rate (ballistic growth at infinite NNN). To explain the behavior of the effective stiffness when $E_{\rm ES} = 0$ [i.e., why in Fig. 5 the green (with upward-pointing triangles) curves exhibits essentially the same behavior as the unstable case [blue (with downward-pointing triangles) curve] with F], because in that case there is no instability (and thus no wavelength). We think that as long as attachment is fast (and the equilibrium concentration at step edges vanishes), we are simply probing the fluctuations in the diffusion field at the step edge: Since the flux of diffusing adatoms reaching the step is essentially $D_T c^{\rm eq}/\ell = F\ell$, the fractional fluctuations of this quantity are proportional to its square root, and thus to $F^{-1/2}$, which is exactly what we measure.

[5]Krug *et al.* [39] demonstrated that, under certain conditions (in the low-temperature limit $2E_1/k_BT \gg 1$ for vicinal surfaces with small surface slopes $u = \partial h/\partial x \sim 0$, a regime not easily accessed in experiment but readily probed in simulations), the mobility and the stiffness are found to be quadratic and inversely proportional to the overall surface slope: $\sigma \sim u^2$ and $\tilde{\beta} \sim |u|^{-1}$, respectively. Thus, if the flux dependence of one of these quantities is known, one may deduce, *heuristically*, the corresponding approximated dependence of the two others. For example, for $u \sim F^{1/2}$, one deduces $\sigma \sim F$ and $\tilde{\beta} \sim F^{-1/2}$. These behaviors are consistent with the overall behavior of the effective stiffness and the adatom mobility found in our simulations with only NN interactions. Note that $\sigma \sim F$ is also in agreement with Ref. [40] (see Fig. 8 for the step velocity; the step mobility is then almost linear with F in our range of flux.

V. CONCLUSION

We have performed extensive kMC simulations to understand how the meandering-instability wavelength, the effective stiffness, and the effective mobility depend on the deposition rate F and the NNN interaction strength. We found excellent agreement with the experimental values of the wavelength on copper when NNN interactions are taken into account in our simulations. Our simulations determine the "exact" behavior of the effective stiffness as functions of the deposition rate and how it relates to the meandering wavelength in the unstable regime; both of them show strong decrease with increasing NNN interaction strength.

In the unstable regime, the effective meandering wavelength is argued to be a manifestation of the competition between the effective step stiffness and the adatom mobility, which are both presumed to depend on the deposition rate. The stiffness exhibits the F power laws: $\tilde{\beta}_{\rm eff} \sim F^{-p}$; leading to a meandering wavelength $\lambda_{\rm eff} \sim F^{-q}$ with $q \approx p/2$, i.e., roughly half of the stiffness exponent. Moreover, $q = q(E_2)$, rather than a constant value $q = 1/2$ as predicted by linear stability analysis. As shown above, p (then q) is found to be related to the kinetics of attachment at step edges: p increases when the kinetics is fast; likewise we can say p decreases with the NNN interaction strength. Thus, the stiffness becomes less dependent on the flux with increasing NNN interaction energy E_2: the exponent p is reduced by a factor close to 3 (from 0.95 to 0.33). Simultaneously, the wavelength becomes less dependent on the flux, since the exponent q is decreased from 0.45 to 0.17, also reduced by a factor close to 3.

Finally, we emphasize that the obtained instability wavelength is an alternative form of meandering instability which we term "roughening-limited" growth, rather than attachment-detachment-limited growth that governs the BZ instability. For NN interactions only, the attachment process is balanced by the detachment process ("the most significant transitions involve the motion of atoms along terraces and step edges which result in diffusion of adatoms and edge adatoms" [20,41]); this smoothing effect allows steps to fluctuate nearly in phase. However, the inclusion of NNN interactions enhances step roughening, inhibiting the growth of the meandering wavelength (impurities probably produce a similar effect). In conclusion, NNN interactions seem to induce competing effects between the instability (whose main mechanism is the Ehrlich-Schwoebel barrier) and the step dynamics (whose main mechanism is step kinetics and incoming deposition

rate), leading to the obtained wavelength behavior vs F; i.e., the exponent q depends now on the strength of NNN interactions.

Good quantitative agreement is found for most of the experimental results presented in Ref. [5]. However, no formal analysis exists of how NNN interaction or other mechanisms (such as impurities) might lead to crossover of the exponent q from its BZ value. Our simulation results may be fruitful for developing improved theories of step instabilities. The precise measurement of adatom mobility is a complicated task. While a detailed analysis of the surface diffusion problem is certainly warranted, such an investigation exceeds the scope of this paper.

ACKNOWLEDGMENTS

We thank L. Douillard for sharing more details about experimental results of Ref. [5] and A. Pimpinelli for many fruitful discussions. Work at University of Maryland was supported in part by NSF (USA) Grant No. CHE 13-05892.

[1] J. Stangl, V. Holy, and G. Bauer, Rev. Mod. Phys. **76**, 725 (2004).
[2] O. Pierre-Louis, C. Misbah, Y. Saito, J. Krug, and P. Politi, Phys. Rev. Lett. **80**, 4221 (1998).
[3] O. Pierre-Louis, M. R. D'Orsogna, and T. L. Einstein, Phys. Rev. Lett. **82**, 3661 (1999).
[4] F. Nita and A. Pimpinelli, Phys. Rev. Lett. **95**, 106104 (2005).
[5] T. Maroutian, L. Douillard, and H.-J.Ernst, Phys. Rev. B **64**, 165401 (2001).
[6] N. Néel, T. Maroutian, L. Douillard, and H.-J. Ernst, Phys. Rev. Lett. **91**, 226103 (2003); J. Phys.: Condens. Matter **15**, S3227 (2003).
[7] T. Maroutian, L. Douillard, and H.-J. Ernst, Phys. Rev. Lett. **83**, 4353 (1999).
[8] H. Mehl, O. Biham, I. Furman, and M. Karimi, Phys. Rev. B **60**, 2106 (1999); T. L. Einstein, J. Jacobsen, and C. Schiff, The Bull. Am. Phys. Soc. abstract is online at http://flux.aps.org/meetings/YR97/BAPSMAR97/abs/S170003.html.
[9] A. Ben-Hamouda, N. Absi, P. E. Hoggan, and A. Pimpinelli, Phys. Rev. B **77**, 245430 (2008).
[10] A. BH. Hamouda, A. Pimpinelli, and R. J. Phaneuf, Surf. Sci. **602**, 2819 (2008).
[11] A. BH. Hamouda, R. Sathiyanarayanan, A. Pimpinelli, and T. L. Einstein, Phys. Rev. B **83**, 035423 (2011).
[12] A. BH. Hamouda, A. Pimpinelli, and T. L. Einstein, Europhys. Lett. **88**, 26005 (2009).
[13] R. L. Schwoebel, J. Appl. Phys. **40**, 614 (1969).
[14] Y. Shim and J. G. Amar, Phys. Rev. B. **73**, 035423 (2006).
[15] H. J. W. Zandvliet, R. Van Moere, and B. Poelsema, Phys. Rev. B. **68**, 073404 (2003).
[16] M. Rusanen, I. T. Koponen, J. Heinonen, and T. Ala-Nissila, Phys. Rev. Lett. **86**, 5317 (2001).
[17] L. Douillard, Habilitation à diriger des recherches "Nanostructures, de l'élaboration aux propriétés," Université Pierre et Marie Curie—Paris VI, 2010; http://iramis.cea.fr/Pisp/ludovic.douillard/.
[18] R. Gerlach, T. Maroutian, L. Douillard, D. Martinotti, and H.-J. Ernst, Surf. Sci. **480/3**, 97 (2001).
[19] J. Kallunki and J. Krug, Phys. Rev. E **62**, 6229 (2000).
[20] J. Kallunki, Growth instabilities of vicinal crystal surfaces during molecular beam epitaxy, Ph.D. dissertation, Universität Duisburg-Essen, 2003, duepublico.uni-duisburg-essen.de/servlets/DerivateServlet/Derivate-11769.
[21] M. Karimi, T. Tomkowski, G. Vidali, and O. Biham, Phys. Rev. B **52**, 5364 (1995).
[22] S. Islamuddin Shah, G. Nandipati, A. Karimand, and T. S. Rahman, J. Phys.: Condens. Matter **28**, 025001 (2016), and references therein.
[23] J. Kallunki, J. Krug, and M. Kotrla, Phys. Rev. B **65**, 205411 (2002).
[24] O. Pierre-Louis and C. Misbah, Phys. Rev. Lett. **76**, 4761 (1996); O. Pierre-Louis, *ibid.* **87**, 106104 (2001).
[25] R. Sathiyanarayanan, Ajmi BH. Hammouda, A. Pimpinelli, and T. L. Einstein, Phys. Rev. B **83**, 035424 (2011).
[26] Ajmi BH. Hamouda, T. J. Stasevich, A. Pimpinelli, and T. L. Einstein, J. Phys.: Condens. Matter **21**, 084215 (2009).
[27] T. Maroutian, Etude expérimentale d'instabilités de croissance des faces vicinales, Ph.D. dissertation, Université Paris 7, 2001; http://www.worldcat.org/title/etude-experimentale-dinstabilites-de-croissance-des-faces-vicinales/oclc/708559063.
[28] J. Krug, Int. Ser. Numer. Math. **149**, 69 (2005).
[29] F. Gillet, O. Pierre-Louis, and C. Misbah, Eur. Phys. J. B **18**, 519 (2000); The authors define two "classes" of adatoms: "Thermal adatoms of concentration c_T detach from a step, diffuse on terraces and re-attach to a step. Mass transport associated to their motion induces relaxation towards equilibrium. The relaxational contribution c_T is a thermal part and is obviously independent of F". "Freshly landed adatoms of concentration c_F have not yet been incorporated into a step."
[30] O. Pierre-Louis and C. Misbah, Phys. Rev. B **58**, 2259 (1998); O. Pierre-Louis, Surf. Sci. **529**, 114 (2003); O. Pierre-Louis, G. Danker, J. Chang, K. Kassner, and C. Misbah, J. Cryst. Growth **275**, 56 (2005).
[31] J. Krug and M. Schimschak, J. Phys. I France **5**, 1065 (1995).
[32] T. J. Stasevich, T. L. Einstein, R. K. P. Zia, M. Giesen, H. Ibach, and F. Szalma, Phys. Rev. B **70**, 245404 (2004); T. J. Stasevich and T. L. Einstein, Multiscale Model. Simul. **6**, 90 (2007).
[33] M. Korner, M. Einax, and P. Maass, Phys. Rev. B **86**, 085403 (2012).
[34] A. Beausoleil, P. Desjardins, and A. Rochefort, Phys. Rev. E **89**, 032406 (2014).
[35] T. J. Stasevich, T. L. Einstein, and S. Stolbov, Phys. Rev. B **73**, 115426 (2006).
[36] Y. Saito and M. Uwaha, Phys. Rev. B **49**, 10677 (1994).
[37] L. Persichetti, A. Sgarlata, M. Fanfoni, M. Bernardi, and A. Balzarotti, Phys. Rev. B **80**, 075315 (2009).
[38] M. Sato, S. Kondo, and M. Uwaha, J. Cryst. Growth **318**, 14 (2011).
[39] J. Krug, H. T. Dobbs, and S. Majaniemi, Z. Phys. B **97**, 281 (1995).
[40] M. Khenner, Phys. Rev. E **88**, 022402 (2013).
[41] R. E. Caflisch, W. E, M. F. Gyure, B. Merriman, and C. Ratsch, Phys. Rev. E **59**, 6879 (1999).